Virology 446 (2013) 162–172

Contents lists available at ScienceDirect

Virology

journal homepage: www.elsevier.com/locate/yviro

Rapid Communication

Biochemical and structural studies of the oligomerization domain of the Nipah virus phosphoprotein: Evidence for an elongated coiled-coil homotrimer

David Blocquel [a,1], Matilde Beltrandi [a,1], Jenny Erales [a], Pascale Barbier [b], Sonia Longhi [a,*]

[a] CNRS and Aix-Marseille Université, Architecture et Fonction des Macromolécules Biologiques (AFMB), UMR 7257, 13288 Marseille, France
[b] Aix-Marseille Université, INSERM, CRO2 UMR_S911, Faculté de Pharmacie, 13385 Marseille, France

ARTICLE INFO

Article history:
Received 15 June 2013
Returned to author for revisions
8 July 2013
Accepted 24 July 2013
Available online 28 August 2013

Keywords:
Henipavirus
Nipah virus
Phosphoprotein
PMD
P multimerization domain
Coiled-coil
Homotrimer
Small-angle X-ray scattering
Cross-linking
Analytical ultracentrifugation

ABSTRACT

Nipah virus (NiV) is a recently emerged severe human pathogen that belongs to the *Henipavirus* genus within the *Paramyxoviridae* family. The NiV genome is encapsidated by the nucleoprotein (N) within a helical nucleocapsid that is the substrate used by the polymerase for transcription and replication. The polymerase is recruited onto the nucleocapsid via its cofactor, the phosphoprotein (P). The NiV P protein has a modular organization, with alternating disordered and ordered domains. Among these latter, is the P multimerization domain (PMD) that was predicted to adopt a coiled-coil conformation. Using both biochemical and biophysical approaches, we show that NiV PMD forms a highly stable and elongated coiled-coil trimer, a finding in striking contrast with respect to the PMDs of *Paramyxoviridae* members investigated so far that were all found to tetramerize. The present results therefore represent the first report of a paramyxoviral P protein forming trimers.

Introduction

The Nipah (NiV) and Hendra (HeV) viruses are recently emerged, severe human pathogens within the *Paramyxoviridae* family (Eaton et al., 2007). A few distinctive properties, including the spectacularly larger size of their phosphoproteins (P), set them aside from other paramyxoviruses and led to their classification within the *Henipavirus* genus of the *Paramyxoviridae* family (Wang et al., 2000). The newly identified Cedar virus has been also classified within this genus (Marsh et al., 2012). The *Henipavirus* genome is encapsidated by the nucleoprotein (N) within a helical nucleocapsid. This helical N:RNA complex, rather than naked RNA, serves as substrate for both transcription and replication. By analogy with other paramyxoviruses, the viral polymerase is thought to consist of the L protein and the P protein. The P protein is an essential polymerase cofactor as it tethers L onto the nucleocapsid template. Beyond its role in recruiting the L protein, P is also thought to serve as a chaperone for N, in that its association prevents illegitimate self-assembly of N (see (Albertini et al., 2005; Blocquel et al., 2012a; Lamb and Parks, 2007; Roux, 2005) for reviews on paramyxovirus transcription and replication). *Henipavirus* N and P proteins were shown to interact with each other (Habchi et al., 2011), being able to form both homologous and heterologous N–P complexes (Blocquel et al., 2012b; Chan et al., 2004; Omi-Furutani et al., 2010).

So far, structural and molecular information on *Henipavirus* proteins is scarce. Indeed high-resolution structural data are limited to their surface proteins, where crystallographic studies led to the determination of the 3D structure of *Henipavirus* fusion and attachment proteins (Bowden et al., 2008a, 2008b, 2010;

Abbreviations: NiV, Nipah virus; HeV, Hendra virus; N, nucleoprotein; L, large protein; P, phosphoprotein; PNT, P N-terminal domain; PCT, P C-terminal domain; PMD, P multimerization domain; XD, X domain of P; MeV, measles virus; SeV, Sendai virus; MuV, mumps virus; RV, rabies virus; VSV, vesicular stomatitis virus; RDV, Rinderpest virus; RSV, respiratory syncytial virus; NMR, nuclear magnetic resonance; PCR, polymerase chain reaction; OD, optical density; IMAC, immobilized metal affinity chromatography; GF, gel filtration; SDS-PAGE, sodium dodecyl sulphate polyacrylamide electrophoresis; R_S, Stokes radius; R_g, radius of gyration; MALDI-TOF, matrix-assisted laser desorption ionization/time of flight; CD, circular dichroism; TFE, 2,2,2-trifluoroethanol; MRE, mean ellipticity values per residue; SAB, Suberic acid bis (*N*-hydroxy-succinimide ester); SAXS, small angle X-ray scattering; T_m, melting temperature

* Corresponding author: AFMB, UMR 7257 CNRS and Aix-Marseille University, 163 avenue de Luminy, Case 932, 13288 Marseille Cedex 09, France.
Fax: +33 4 91 26 67 20.
E-mail address: Sonia.Longhi@afmb.univ-mrs.fr (S. Longhi).

[1] These authors have equally contributed to the work.

0042-6822/$ - see front matter © 2013 Elsevier Inc. All rights reserved.
http://dx.doi.org/10.1016/j.virol.2013.07.031

Lou et al., 2006). The only available molecular data on *Henipavirus* N and P proteins come from our previous studies (Blocquel et al., 2012b; Habchi et al., 2011, 2010). Those studies showed that the N and P proteins possess a modular organization consisting of both ordered and intrinsically disordered regions, where these latter are functional regions that lack highly populated secondary and tertiary structure under physiological conditions in the absence of a partner (for reviews on IDPs, see (Chouard, 2011; Dunker et al., 2008a, 2008b; Turoverov et al., 2010; Uversky, 2010, 2013; Uversky and Dunker, 2010)). *Henipavirus* N proteins were shown to consist of a structured region (N_{CORE}) and of an intrinsically disordered C-terminal region (N_{TAIL}, aa 400–532). Likewise, the P proteins contain an exceptionally long N-terminal disordered region (PNT, aa 1–406 in NiV) (Habchi et al., 2010) and a C-terminal moiety (PCT, aa 407–709 in NiV). While PNT is common to both P and V proteins, with this latter originating from co-transcriptional editing (addition of an extra G nucleotide) of the mRNA of NiV P, PCT is unique to the P protein. PCT has a modular organization being composed of alternating disordered and ordered regions: it embraces a predicted disordered region overlapping the V ORF (aa 407–456 in NiV) referred to as spacer, a structured region (aa 470–578) referred to PMD (for P multimerization domain), a disordered linker (aa 579–659 in NiV) and a globular region (aa 660–709) referred to as X domain (XD) (Fig. 1) (Habchi et al., 2010). Like in the closely related measles (MeV) and Sendai (SeV) viruses (Belle et al., 2008; Bischak et al., 2010; Blanchard et al., 2004; Bourhis et al., 2004, 2005; Gely et al., 2010; Houben et al., 2007; Jensen et al., 2010; Johansson et al., 2003; Kavalenka et al., 2010; Longhi et al., 2003; Morin et al., 2006; Ringkjøbing Jensen et al., 2011), *Henipavirus* X domains adopt an α-helical conformation and were shown to trigger α-helical folding of *Henipavirus* N_{TAIL} (Habchi et al., 2011; Martinho et al., 2012).

The structure of MeV XD has been solved both in the crystal and in solution and was shown to consist of a triple α-helical bundle (Bernard et al., 2009; Johansson et al., 2003). High-resolution structural data are also available for the X domains of the closely related SeV and mumps virus (MuV), the structure of which has been solved by nuclear magnetic resonance (NMR) and X-ray crystallography, respectively (Blanchard et al., 2004; Kingston et al., 2008). Structural data are also available for the C-terminal P domains from *Rhabdoviridae* members, namely rabies virus (RV) (Mavrakis et al., 2004), vesicular stomatitis virus (VSV) (Ribeiro et al., 2008) and Mokola virus (Assenberg et al., 2010). Interestingly, comparison of the P nucleocapsid-binding domains solved so far suggests that the nucleocapsid binding domains are structurally conserved among *Paramyxoviridae* and *Rhabdoviridae* P in spite of low sequence conservation (Delmas et al., 2010).

In *Paramyxovirinae,* sequence analyses predict a coiled-coil region within PMD (Habchi et al., 2010; Karlin et al., 2003) (Fig. 1). In agreement, X-ray crystallography studies showed that SeV, MeV and MuV PMDs are coiled-coil tetramers (Communie et al., 2013; Cox et al., 2013; Tarbouriech et al., 2000b). The tetrameric coiled-coil organization of PMD has also been experimentally confirmed in the case of Rinderpest (RDV) (Rahaman et al., 2004) and respiratory syncytial virus (RSV) (Llorente et al., 2006, 2008). By contrast, the corresponding PMDs of RV and VSV were shown to form dimers with a different structural arrangement (Ding et al., 2006; Ivanov et al., 2010).

The actual oligomeric state of *Henipavirus* P is unknown. As a first step towards the characterization of *Henipavirus* P proteins, we report the expression, purification and characterization of NiV PMD. Using a combination of biochemical and biophysical approaches, we show that PMD forms a homotrimeric coiled-coil structure with an overall elongated shape.

Results and discussion

Cloning, expression and purification of PMD

The P gene fragment encoding PMD was cloned into the pDEST14 plasmid (Invitrogen) to yield a C-terminal histidine-tagged recombinant product, the expression of which is under the control of the T7 promoter. Most PMD was recovered from the soluble fraction of the bacterial lysate (not shown). The protein

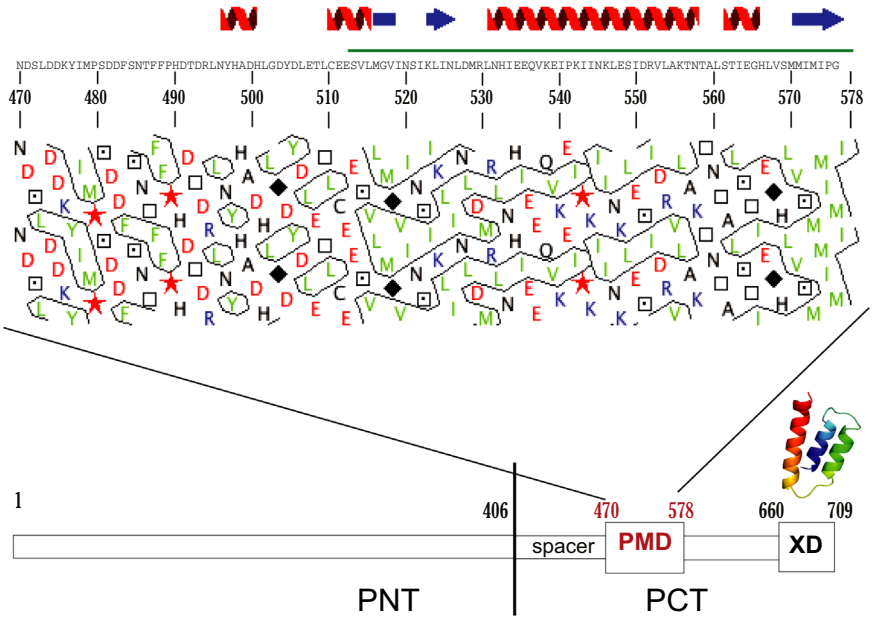

Fig. 1. Domain organization of NiV P. Domain organization of P showing that it is composed of two moieties, PNT (aa 1–406) and PCT (aa 407–709). PCT consists of a disordered region (aa 407–469) referred to as "spacer", a structured region (aa 470–478) referred to PMD for P multimerization domain, a disordered linker (aa 579–659) and a globular region (aa 660–709) referred to as X domain (XD). The HCA plot of PMD, displayed on the top, points out the presence of a region encompassing residues (underlined by a green bar) with the typical texture of a coiled-coil region (see (Ferron et al., 2005)). The ribbon representation of the structural model of NiV XD (Habchi et al., 2011) is shown. The structure was drawn using Pymol (DeLano, 2002).

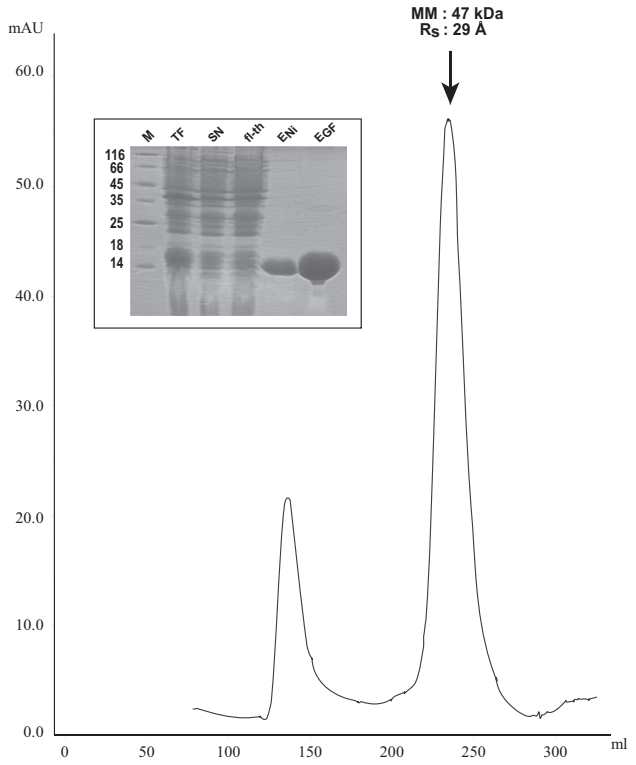

Fig. 2. Elution profile and purification of NiV PMD from gel filtration. The arrows points the peak containing PMD. The corresponding apparent molecular mass (MM) and Stokes radius (R_S) are shown. Inset: Coomassie blue staining of SDS-PAGE showing the bacterial lysate (total fraction, TF), the clarified supernatant (soluble fraction, SN), the unretained fraction (fl-th), the eluent from immobilized metal affinity chromatography (E_{Ni}) and the eluent from gel filtration (E_{GF}). M: molecular mass markers (kDa). All samples were thermally denatured for 5 min prior to electrophoretic migration.

was purified to homogeneity (> 95%) in two steps: IMAC and GF (see inset in Fig. 2). Although the purified protein was found to migrate with an apparent molecular mass slightly higher (16 kDa) than expected from its amino acid sequence (13,475 Da), MALDI-TOF mass spectrometry analysis yielded the expected molecular mass (13,473 Da). In addition, the identity of the purified protein was confirmed by mass spectrometry analysis of the tryptic fragments obtained after digestion of the purified protein band excised from SDS-polyacrylamide gels, which yielded a sequence coverage of 49%.

Hydrodynamic properties and oligomerization state of PMD

Although the gel filtration profile, obtained by injecting the eluent from the IMAC, features two peaks, the protein was consistently found only in the second peak (Fig. 2). In addition, the elution profile was shown to be independent from protein concentration. PMD is eluted as a sharp and symmetric peak, with an apparent molecular mass of 47 kDa (Fig. 2). This value is not consistent with a monomeric form of the protein (13.5 kDa) and could correspond either to a very compact tetramer (54 kDa) or to an elongated trimer (40.5 kDa). The Stokes radius (R_S), as inferred from the apparent molecular mass (Uversky, 2002), is 29 Å, a value close to that expected for a globular trimer (28 Å) (Uversky, 2002).

Intriguingly, when the purified protein was not thermally denatured prior to electrophoretic migration, an additional band of approximately 40 kDa was observed in SDS-PAGE (Fig. 3A). This band, whose mass corresponds to the value expected for a trimeric form, disappears when the protein was subjected to thermal denaturation (Fig. 3A). This observation argues for a very stable oligomer that resists under denaturing conditions (i.e. in spite of the presence of SDS). In addition, when the sample was incubated at 95 °C for 5 min in the absence of SDS and subsequently cooled down to room temperature, it readily recovers it native-like state, as judged from the fact that it migrates again in SDS-PAGE both as a monomer and as a trimer (data not shown). Formation of the PMD oligomer is not mediated by disulphide bridges, as addition of 20 mM DTT does not affect its migration in SDS-PAGE (Fig. 3A).

We then performed cross-linking experiments using SAB, a bifunctional reagent of fixed size (13.1 Å) that reacts with lysine. As shown in Fig. 3B, increasing cross-linker concentrations readily resulted in the appearance of a dimeric form, along with that of a trimer when higher cross-linker concentrations were used. Further increasing the SAB concentration up to 10 mM did not result in further accumulation of the trimeric form (data not shown). At a SAB concentration of 1 mM and, most of all, of 3.3 mM, a smear becomes detectable above the band of the trimer, which might allude to a very faint and hardly detectable band of higher (66 kDa) molecular mass. Note however that when similar experiments were performed with tetrameric MuV, RPV and SeV PMDs, a clear and discrete band corresponding to the tetrameric form could be readily detected (Cox et al., 2013; Rahaman et al., 2004; Tarbouriech et al., 2000b). Although the present cross-linking experiments on their own are not sufficient to draw definite conclusions about the oligomeric state of NiV PMD, these experiments, together with the migration behavior of the protein on a denaturing gel, are first clues that this domain could be a trimer. Based on these observations, the experimentally observed GF profile, reflecting either an extended trimer or a compact tetramer, more likely can be ascribed to an elongated trimer. In further support of this, an apparent molecular mass larger than expected was also observed in the GF profiles of the cognate SeV and RDV PMDs, a behavior that was ascribed to their elongated coiled-coil conformation (Rahaman et al., 2004; Tarbouriech et al., 2000a). Therefore, since a coiled-coil is also predicted in NiV PMD (Fig. 1), we conclude that this latter can be an elongated trimer.

Sedimentation analysis

To further confirm the trimeric state of NiV PMD, we performed sedimentation velocity experiments at 20 °C. This approach, which is widely used to characterize complex macromolecular interactions and assemblies, has been successfully used to investigate the oligomeric state in solution of PMD from related viruses (for examples see (Cox et al., 2013; Llorente et al., 2008)).

The $C(S)$ function revealed the presence of a predominant species, corresponding to 91% of the loaded concentration, which sediments at 3.7 ± 0.3 S (Fig. 4A). The molecular mass derived from this sedimentation coefficient (Fig. 4B) is equal to 43 kDa, a value close to the expected molecular mass of a trimer (40.5 kDa). The second species that represent only 9%, sedimented at 5.3 ± 0.3 S and its molecular mass is approximately 76 kDa. This latter minor form can reflect either a higher-order oligomer or an aggregated form.

We also used sedimentation equilibrium to confirm the oligomeric state of NiV PMD (Fig. 4C). Sedimentation equilibrium was performed with various loading protein concentrations (1.9, 2.0 and 2.5 mg/mL) at 10,000, 12,000, 17,000 and 40,000 rpm at 4 °C. Analysis of the data showed a best residuals distribution for a single species model. However, the molecular mass obtained at 280 nm weakly decreased when the speed increased indicating the presence of some other non-interacting species, in agreement with the sedimentation velocity data (peak at 5.3 S). When all the data were taken into account, the obtained molecular mass was $44{,}500 \pm 4000$ Da. However, the value obtained at 257 nm was

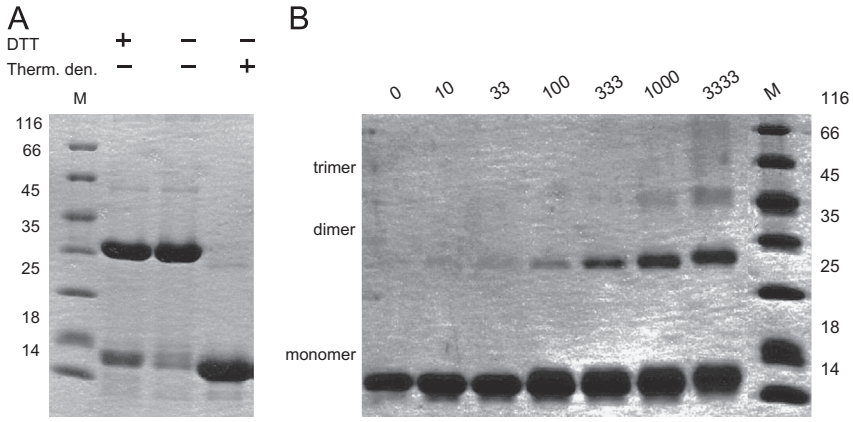

Fig. 3. Effect of thermal denaturation and cross-linking experiments. (A) Coomassie stained 15% SDS-PAGE showing the electrophoretic migration of purified NiV PMD as obtained either with or without a 5-min thermal denaturation at 95 °C. The migration of a NiV PMD sample not subjected to thermal denaturation and containing 20 mM DTT is also shown. (B) Coomassie stained 15% SDS-PAGE showing the results of cross-linking with SAB (see "Materials and methods" section). The concentration of SAB (μM) is indicated above the gel. M: molecular mass markers (kDa). Samples were thermally denatured for 5 min prior to electrophoretic migration.

more reliable, especially at high speed where all traces of aggregates are removed. At this wavelength, and considering the different concentrations, the molecular mass was 38,900 ± 900 Da, a value close to that expected for a trimer. We therefore concluded by equilibrium and velocity sedimentation analytical ultracentrifugation, that NiV PMD adopts a trimeric conformation in solution.

Far-UV CD studies of PMD

The nature of the interactions within PMD trimers was investigated using far-UV spectroscopy. The spectrum of PMD is indicative of a folded protein with a high α-helical content (Fig. 5A). In agreement, spectra deconvolution led to an estimated α-helical content of roughly 65% (see inset in Fig. 5A). Interestingly, the ratio of the ellipticities at 222 and 208 nm ($\Theta_{222/208}$) is greater than 1.0 (Fig. 5A), a property indicative of the presence of interacting helices and also already observed in the case of PMDs from SeV (Tarbouriech et al., 2000a), RDV (Rahaman et al., 2004) and MeV (Blocquel et al., unpublished data). Notably, although upon addition of increasing concentrations (50–80%) of TFE no dramatic variation in the secondary structure content was observed, the $\Theta_{222/208}$ ratio drops below 1, a characteristic of non-interacting α-helices (Fig. 5A and data not shown). Because high TFE concentrations are known to disrupt tertiary and quaternary structure and to stabilize secondary structure (Lau et al., 1984), these results suggest that NiV PMD forms trimers through coiled-coil interactions.

To further investigate the thermal stability of PMD trimers, we recorded the CD spectrum at 100 °C along with that obtained upon a stepwise cooling down to 20 °C (Fig. 5A). We also monitored the mean residue ellipticity at 222 nm (MRE_{222}), indicative of the α-helical content, at increasing temperatures and plotted it as a function of temperature (Fig. 5B). The unfolding profile shows two cooperative transitions (Fig. 5B). In particular, a gradual, yet low, reduction in the intensity of MRE_{222} is observed when the sample is heated from 20 °C up to 40 °C, temperature above which a steep transition occurs (Fig. 5B). At approximately 70 °C an inflexion point is observed, which is followed by a second steep transition (Fig. 5B). Support for a two-transitions profile comes from comparison between experimental data and data fitted to a two-state thermal unfolding, which shows significant residual values (see inset in Fig. 5B). The plot of residuals indicates the difference between the experimental and reference data for each point in the fit, where a good fit between experimental and reference data has small residuals that randomly distribute around the *X*-axis. The very poor quality of the fit argues for a two-transitions profile (see inset in Fig. 5B). Analysis of the thermal unfolding profile on its whole yielded an apparent melting temperature (T_m) of 76 °C. Individual analysis of the first and second transition yielded an apparent T_m of 52 and 85 °C, respectively (Fig. S1). The observed profile is typical of a three-state cooperative thermal unfolding involving a native state, an intermediate state and an unfolded state. It is tempting to speculate that the first transition could reflect dissociation of the trimer, whereas the second one could correspond to α-helical unfolding.

Following a stepwise cooling from 100 °C down to 20 °C, the final MRE_{222} at 20 °C is close to that of the initial spectrum before heating, which points out the reversibility of thermal unfolding and argues for refolding of the main structural motif (i.e. coiled-coil) (Fig. 5B). In spite of this reversibility, the renaturation curve was found not to be superimposable onto the denaturation curve, indicating different temperature-induced denaturation–renaturation paths (Fig. 5B).

Based on these results, we propose that NiV PMD forms a coiled-coil trimer that displays a high thermal stability, in agreement with the well-established rigid nature of coiled coils (Lupas and Gruber, 2005).

SAXS studies of PMD

SAXS studies are particularly well adapted to study flexible and/or extended macromolecules in solution. They provide low-resolution structural data, and give access to the mean particle size (R_g) as well as to the maximal intramolecular distance (D_{max}). These two parameters give information on the degree of compactness of the molecule, and the latter gives an idea of the maximal degree of extension reached by the molecule in solution. In order to achieve insights into the shape of NiV PMD in solution, we performed SAXS studies. The shapes of the SAXS curves (Fig. 6A) and the Guinier plots obtained (Fig. 6B) are independent of protein concentration, indicating the absence of significant aggregation. Each curve can be well approximated by a straight line in the Guinier region ($q \times R_g < 1.0$). The slope gives the value of the radius of gyration, R_g, while the intercept of the straight line gives the $I(0)$ which is proportional to the molecular mass of the scatterer. Guinier analysis in the low q region gave an R_g of 50.8 ± 0.7 Å, in agreement with the value of 50.2 ± 0.1 Å determined from the pair distribution function $P(r)$ (see Tables 1 and 2). The deduced molecular mass is 41.6 kDa, which is in good agreement with the molecular mass expected for a trimeric form (40.5 kDa) (see Table 1).

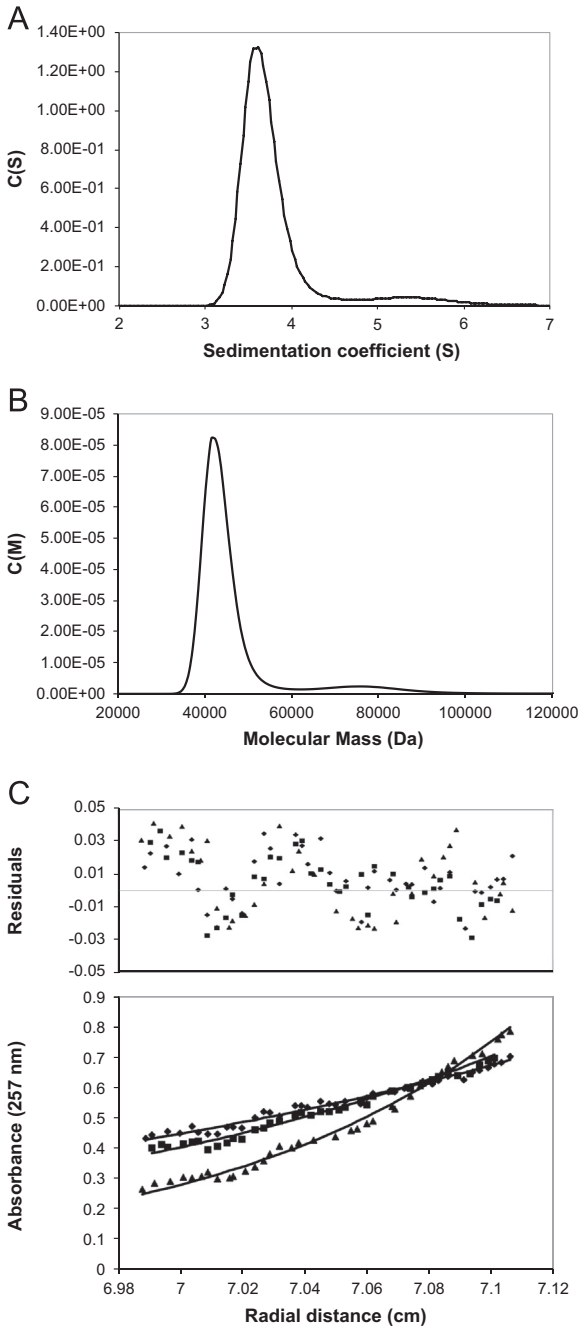

Fig. 4. Sedimentation velocity analysis by SEDFIT program of NiV PMD at 1.9 mg/mL and at 20 °C. (A) The *C*(S) distribution function shows a principally sedimenting species with a sedimentation coefficient of 3.7 S. (B) The *C*(M) distribution function indicates that the above sedimenting species has a molecular weight of 43 kDa, a value close to that expected for a trimeric form of the protein. (C) Sedimentation equilibrium analysis of NiV PMD at 2.5 mg/mL and at 4 °C. The symbols show the experimental radial distribution of NiV PMD at 10,000 rpm (♦), 12,000 rpm (■) and 17,000 rpm (▲). The solid lines represent the best fit curves of analysis with a single species model.

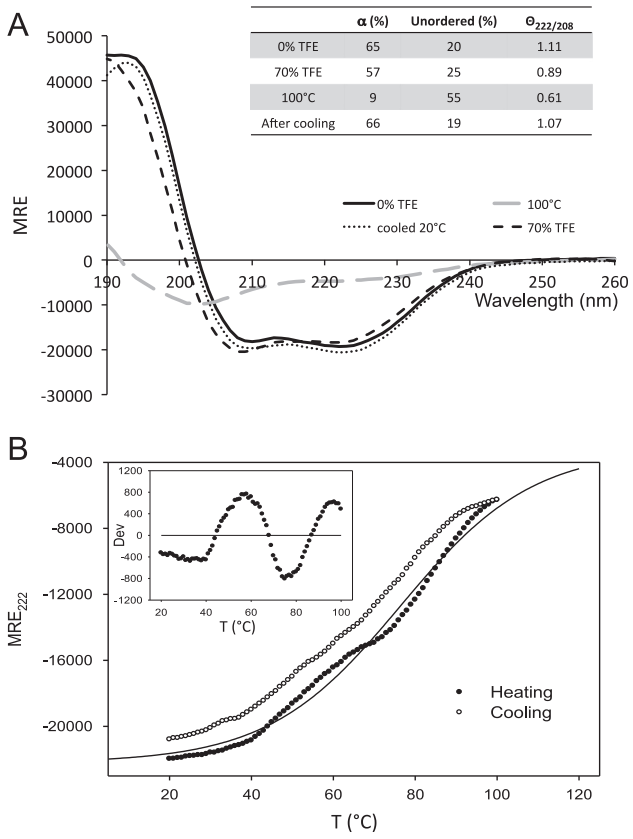

Fig. 5. Analysis of NiV PMD by far-UV circular dichroism. (A) Far-UV CD spectra of NiV PMD at 0.1 mg/mL in 10 mM sodium phosphate pH 7 in the absence (black line) or presence (dashed line) of 70% TFE at 20 °C. The CD spectra obtained at 100 °C (grey line) and after cooling at 20 °C (dotted line) are also shown. The inset shows the relative secondary structure content along with the ellipticity ratio at 222 and 208 nm ($\Theta_{222/208}$). (B) Mean residue ellipticity at 222 nm (MRE_{222} in deg/cm^2/dmol) of NiV PMD as a function of the temperature. Protein and buffer concentrations were the same as described in (A). Full and empty circles show the variation of MRE_{222} during heating and cooling, respectively. The thin black line corresponds to the fitting of experimental data to a sigmoidal curve, as expected for a two-state cooperative transition. The inset shows the plot of residuals between experimental and fitted data. Data are representative of one out two independent experiments.

The experimentally observed R_g value (50.8 Å) is much larger than that expected (22 Å) for a globular protein with an R_s equal to that experimentally observed in the case of NiV PMD (Wilkins et al., 1999). It is even much higher than the value expected (12.0 Å) for a sphere with an R_S of 15.5 Å, as determined from the volume of a sphere with 116 residues (see "Materials and methods" section). The strong discrepancy between the experimentally observed R_g and the value expected for a globular/spherical form indicates that the overall structure of NiV PMD is elongated. This property confirms that the higher apparent molecular mass observed upon GF does reflect an elongated trimer.

The distances distribution function inferred from the scattering curve of PMD exhibits a maximum at 25 Å, a shoulder at 90 Å and a long tail up to 182 Å (D_{max}) typical of an elongated object (Fig. 6C).

The Kratky plot presents a maximum at 8.5 Å and a flat region above 20 Å (Fig. 6D). The shape of the plot is indicative of a structured protein with possibly an at least partly disordered appendage, as judged from the bell-shape nature of the curve that displays a clear maximum and from the presence of the flat region.

Next, we employed the program DAMMIF to carry out ab initio shape reconstruction from the SAXS data. Several series of independent runs were carried out either with no forced symmetry or by imposing P2, P3 or P4 symmetries. Within each symmetry class, models were very reproducible with an average normalized spatial discrepancy (NSD) below 1.0, indicating structurally similar solutions. All generated bead models appeared as elongated cylinders, compatible with a coiled-coil structure. Best results were obtained with the P3 symmetry, as judged from the DAMMIF χ parameter and from the quality of the fit to the experimental curve. Assuming this symmetry, the models resulting from 20 independent DAMMIF runs were superimposed using the DAMAVER suite, which yielded an average

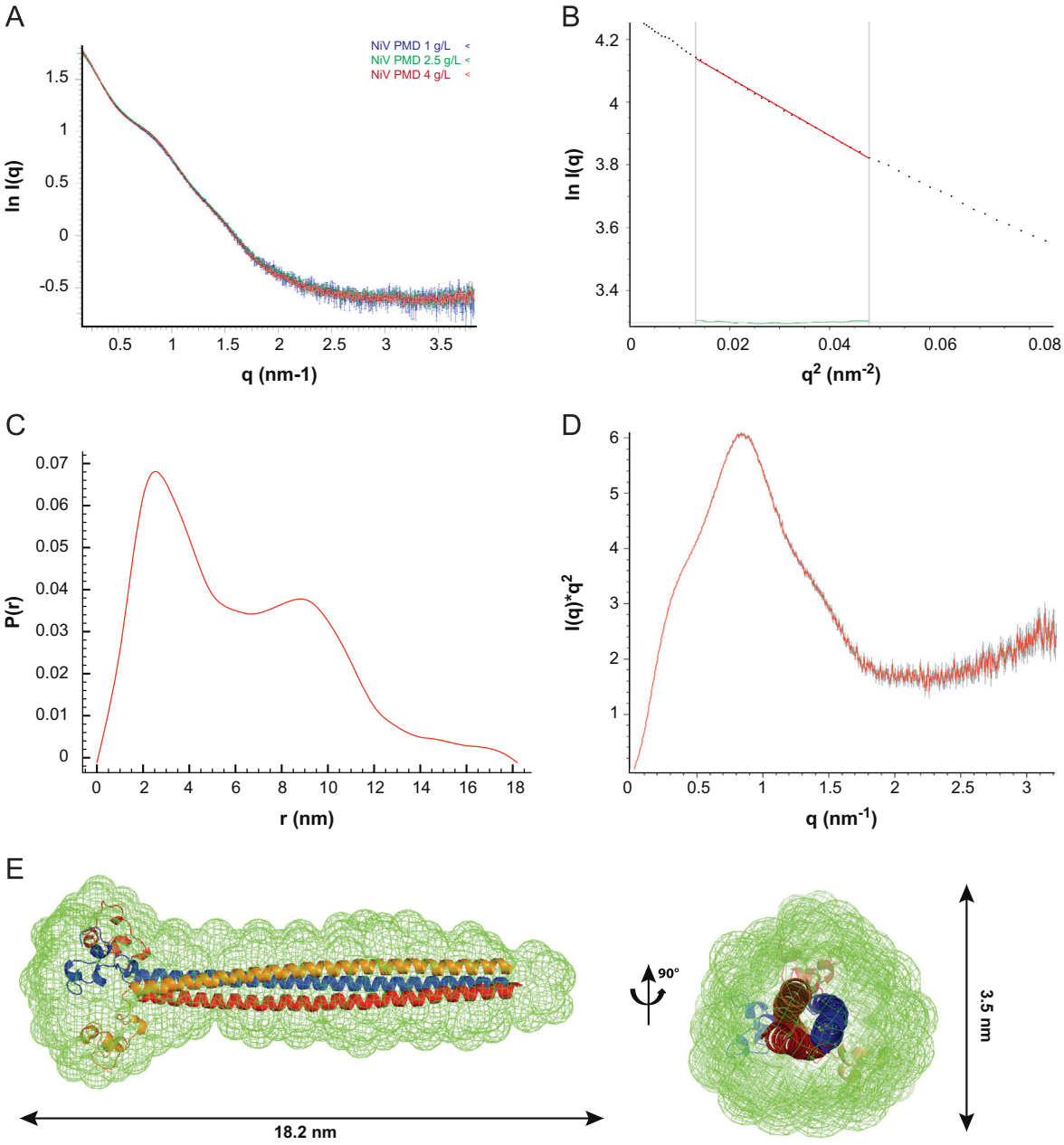

Fig. 6. Small-angle X-ray scattering experiments. (A) Experimental SAXS data recorded for q values up to 3.5 nm^{-1}. The curves obtained for tree protein concentrations (1 mg/mL, blue; 2.5 mg/mL, green; and 4 mg/mL, red) are represented after correction for concentration. (B) Representation of the Guinier plot for the protein at 4 mg/mL. (C) Pair distance distribution, $P(r)$, function of the data for the 4 mg/mL concentration. (D) Kratky plot. (E) Two orthogonal views of the ab initio envelope calculated with DAMAVER (Volkov and Svergun, 2003). The 20 DAMMIF calculations (Franke and Svergun, 2009) were performed and averaged with DAMAVER to produce the averaged and filtered shape show in green. The structure of a putative model of NiV PMD adopting a trimeric coiled-coil conformation with a short N-terminal helical region is shown, with the three chains being displayed in three different colors. Docking of the model in the envelope was done manually using the program Pymol (DeLano, 2002). The structural model fits well in the density of the SAXS-derived model.

NSD of 0.89 ± 0.16. The average filtered model generated by DAMAVER has an elongated shape (Fig. 6E).

We also generated a trimeric coiled-coil model of NiV PMD based on structural predictions that predict a coiled-coil from residue 511 to residue 579 and a helical region upstream (see "Materials and methods" section). The resulting model, which is only a plausible representation and in no way pretends to provide an accurate description of the actual NiV PMD structure, can easily be accommodated in the SAXS envelope (Fig. 6E).

The R_g of a thin rod of length $L = 182$ Å is 52 Å (see "Materials and methods" section), a value in very good agreement with the value estimated from both the Guinier plot and the pair distribution function. Although the overall shape of the model is elongated, the density broadens at one extremity, which could indicate the presence of flexible termini.

To investigate the relevance of our trimeric model, we generated three alternative models corresponding to a monomeric, dimeric and tetrameric form of NiV PMD (see "Materials and methods" section). The program CRYSOL (Svergun et al., 1995) was used to calculate a theoretical SAXS profile from each model, which was then compared to the experimental SAXS profile (Fig. S2). As we used models and not crystal structures, the best fit was observed in the lower values of q (0–1.5 nm^{-1}), which represent the global shape of NiV PMD, whatever the model used

Table 1
SAXS data-collection and scattering-derived parameters.

Data-collection parameters	
Detector	Pilatus (1 M)
Beam geometry	Bending magnet (BM29)
Wavelength (Å)	0.992
q Range ($Å^{-1}$)	0.028–4.525
Exposure time (s)	1
Concentration range (mg/mL)	1–4
Temperature (°C)	10
Structural parameters*	
$I(0)$ (cm^{-1}) (from $P(r)$)	43.8 ± 0.1
R_g (Å) (from $P(r)$)	50.2 ± 0.1
$I(0)$ (cm^{-1}) (from Guinier)	42.7 ± 0.5
R_g (Å) (from Guinier)	50.8 ± 0.7
D_{max} (Å)	182
Molecular-mass determination (kDa)	
Molecular mass (MM) (from $I(0)$)	41.6
Calculated MM from sequence	40.5
Software employed	
Primary data reduction	PRIMUS
Data processing	GNOM
Ab initio analysis	DAMMIF
Validation and averaging	DAMAVER
Three-dimensional graphics representations	*PyMOL*

* Reported for 4 mg/mL measurement.

Table 2
Molecular dimensions of NiV PMD calculated from SAXS experiments.

Protein concentration (mg/mL)	R_g (Å) (Guinier)	$I(0)$ (Guinier) (cm^{-1})	D_{max} (Å)
1	48.2 ± 0.1	41.9 ± 0.5	182
2.5	49.5 ± 0.8	42.4 ± 0.4	184
4	50.8 ± 0.7	42.7 ± 0.5	182

(see insets in Fig. S2). Higher χ values were thus obtained for 2.5 and 4 g/L showing the limit of our model at higher resolution (see insets in Fig. S2). The calculated scattering profile of the trimeric model was found to systematically fit better than that of the other models, especially in the low q values (Fig. S2). Comparisons between calculated and experimental data showed that the trimeric model yields the lowest χ values (see insets in Fig. S2). This analysis affords additional validity to our model of a trimeric organization of NiV PMD.

Conclusions

The present biochemical, biophysical and spectroscopic data indicate that NiV PMD adopts a trimeric, coiled-coil structure in solution. This finding is in striking contrast with what was observed for the closely related SeV, MuV, RDV and MeV, and for RSV, whose PMDs were found to assemble into tetramers (Communie et al., 2013; Cox et al., 2013; Llorente et al., 2006, 2008; Rahaman et al., 2004; Tarbouriech et al., 2000b). The present data not only provide the first experimental evidence that NiV P is a trimer, but also constitute the first report of a paramyxoviral P protein forming trimers. The trimeric nature of NiV P constitutes an additional distinctive property that sets aside *Henipavirus* P proteins from other paramyxoviral P proteins.

Biochemical and structural data gathered so far on *Paramyxoviridae* and *Rhabdoviridae* P proteins indicate that their mutlimerization is a conserved feature in spite of sequence diversity, which implies a functional role. So far, the generally accepted model of polymerase progression along the nucleocapsid template in *Mononegavirales* members posits that the L–P complex cartwheels on the nucleocapsid template via dynamic making and breaking of the N–P interaction (Curran and Kolakofsky, 1999; Kolakofsky et al., 2004). The corollary of this model is a strict requirement for P multimerization. The fact that in *Paramyxoviridae* members, P multimerization relies on coiled-coils, which are known to be extremely mechanically rigid structures, further underscores that P multimerization plays an important functional role. Surprisingly, in the case of rabies virus (see (Leyrat et al., 2010) and references therein cited), the multimerization of P was shown to be dispensable for transcription (Jacob et al., 2001). This finding, together with the rather high affinity between the N and P proteins, led to an alternative model, referred to as "jumping". According to this model, binding and release of P would not be required for transcription and replication: the P protein would be permanently bound to the nucleocapsid template and the polymerase would jump between adjacent P molecules.

The finding that the NiV P multimerization domain adopts a coiled-coil trimeric structure argues for a cartwheeling mechanism, although definite answers await additional functional studies aimed at precisely assessing the role of P multimerization. The trimeric nature of NiV P, which constitutes so far a unique property among *Paramyxoviridae* P proteins, suggests that these latter have evolved from a common ancestor and then diverged in their sequence properties leading to either trimeric or tetrameric assemblies.

The present study is expected to pave the way towards future functional studies aimed at precisely assessing the role of P multimerization, as well as at evaluating the functional impact of varying its oligomeric nature. As such, the results herein presented should engender a renewed interest in the field that ultimately should greatly improve our understanding of the replicative machinery of paramyxoviruses.

Funding

This work was carried out with the financial support of the Agence Nationale de la Recherche, specific programs "Physico-Chimie du Vivant" (ANR-08-PCVI-0020–01). D.B. is supported by a joint doctoral fellowship from the Direction Générale de l'Armement (DGA) and the CNRS. M.B. is partly supported by an Erasmus Master2 fellowship from the University of Milan. J.E. is supported by a post-doctoral fellowship by the Fondation pour la Recherche Médicale (FRM). The funders had no role in study design, data collection and analysis, decision to publish, or preparation of the manuscript.

Materials and methods

Cloning of the PMD coding region

The PMD gene construct, encoding residues 470–578 of the NiV P protein (sequence accession number VaZy2 in the VaZyMolO data base (Ferron et al., 2005)) with an hexahistidine tag fused to its C-terminus, was obtained by PCR, using a synthetic NiV P gene (GenScript), optimized for the expression in *Escherichia coli* as template, and *Pfu* polymerase (Promega). Primers (Operon) were designed to introduce an *AttB1* and *AttB2* sites at the 5′ and 3′ ends, respectively, and to amplify the desired part of the P ORF with a fragment encoding a C-terminal hexahistidine tag. After digestion with *Dpn*I (New England Biolabs) to remove the methylated DNA template, the PCR product was purified (PCR Purification Kit, Qiagen) and cloned into the pDEST14 vector (Invitrogen) using the Gateway® recombination system (Invitrogen). This vector drives the expression of recombinant products under the control of the T7 promoter. Selection and amplification of the

construct was carried out using $CaCl_2$-competent *E. coli* TAM1 cells (Active Motif). The sequence of the coding region of the construct was checked by sequencing (GATC Biotech) and found to conform to expectations.

Expression and purification of PMD constructs

The *E. coli* strain Rosetta [DE3] pLysS (Novagen) was used for expression. The pLysS (Novagen) plasmid carries the lysozyme gene, thus allowing a tight regulation of the expression of the recombinant gene, as well as a facilitated lysis. Cultures were grown overnight to saturation in LB medium containing 100 μg/mL ampicilin and 34 μg/mL chloramphenicol. An aliquot of the overnight culture was diluted 1/25 in LB medium and grown at 37 °C. At OD_{600} of 0.7, isopropyl ß-D-thiogalactopyranoside was added to a final concentration of 0.2 mM, and the cells were grown at 37 °C for 3.5 h. The induced cells were harvested, washed and collected by centrifugation (5000*g*, 10 min). The resulting bacterial pellets were frozen at −20 °C.

The pellet containing PMD was resuspended in 5 volumes (v/w) buffer A (50 mM Tris/HCl pH 8, 300 mM NaCl, 20 mM Imidazole, 1 mM phenyl-methyl-sulphonyl-fluoride (PMSF)) supplemented with 0.1 mg/mL lysozyme, 10 μg/mL DNAse I, 20 mM $MgSO_4$ and protease inhibitor cocktail (Sigma) (one tablet for 2 L-culture). After a 20-min incubation with gentle agitation, the cells were disrupted by sonication (using a 750 W sonicator and five cycles of 30 s each at 60% power output). The lysate was clarified by centrifugation at 30,000*g* for 30 min and then purified by immobilized metal affinity chromatography (IMAC). Starting from a 1 L culture, the clarified supernatant was injected onto a 5-mL HisTrap FF column (GE, Healthcare), previously equilibrated in buffer A supplemented with 1 M NaCl. Elution was carried out using a gradient of imidazole (20–500 mM) in buffer A supplemented with 1 M NaCl. Eluents were analyzed by SDS-PAGE for the presence of the desired product. The fractions containing PMD were combined and loaded onto a Superdex 200 26/60 column (GE, Healthcare) and eluted in 20 mM Tris/HCl pH 8, 5 mM EDTA and 150 mM NaCl. Proteins were concentrated using Centricon Plus-20 (molecular cutoff of 3000 Da) (Millipore) and then stored at −20 °C.

All purification steps, except for IMAC and gel filtrations (GF), were carried out at 4 °C. Apparent molecular mass of proteins eluted from the gel filtration column was deduced from a calibration carried out with LMW and HMW calibration kits (Amersham Pharmacia Biotech).

Protein concentrations were calculated using a theoretical absorption coefficient at 280 nm of 0.332 mg/mL/cm, as obtained using the program ProtParam at the EXPASY server (http://www.expasy.ch/tools).

Mass spectrometry (MALDI-TOF)

Mass analysis of the purified PMD protein was performed using an Autoflex II TOF/TOF. Spectra were acquired in the linear mode. Samples (0.7 μL containing 15 pmol) were mixed with an equal volume of sinapinic acid matrix solution, spotted on the target, then dried at room temperature for 10 min. The mass standard was myoglobin. Proteins were analyzed in the Autoflex matrix-assisted laser desorption ionization/time of flight (MALDI-TOF) (Bruker Daltonics, Bremen, Germany).

The identity of the purified PMD protein was confirmed by mass spectral analysis of tryptic fragments. The latter was obtained by digesting (0.25 μg trypsin) 1 μg of purified recombinant protein obtained after separation onto SDS-PAGE. The tryptic peptides were analyzed as described above and peptide fingerprints were obtained and compared with *in-silico* protein digest (Biotools, Bruker Daltonics, Germany). The mass standards were either autolytic tryptic peptides or peptide standards (Bruker Daltonics).

Calculation of the hydrodynamic radius and of radius of gyration

The theoretical Stokes radii (R_S, in Å) expected for a natively folded (R_S^{NF}) protein with an expected molecular mass (MMtheo) (in Daltons) was calculated according to Uversky (2002):

$$\log(R_s^{NF}) = 0.369\ \log(\mathrm{MMtheo}) - 0.254 \quad (1)$$

The theoretical Stokes radii (R_S) of a natively folded trimer (R_S^{Trimer}) was calculated as:

$$\log(R_s^{\mathrm{Trimer}}) = 0.369\ \log(\mathrm{MMtheo} \times 3) - 0.254 \quad (2)$$

The theoretical radius of gyration (R_g, in Å) expected for a globular protein with a hydrodynamic radius R_S was calculated according to Wilkins et al. (1999):

$$R_g = (3/5)^{1/2} R_S \quad (3)$$

The R_g of a thin rod with a length L can be calculated as:

$$R_g^2 = L^2/12 \quad (4)$$

NiV PMD consists of 116 residues, including the initial methionine and the hexahistidine tag. Using an average volume of 134 $Å^3$ per residue for proteins, the radius of a sphere with that volume $V = 4/3\ \pi R_S^3$ would be $R_S = 15.5$ Å. According to Eq. (3), its corresponding R_g, is 12.0 Å.

Analytical ultracentrifugation

Sedimentation velocity experiments were carried out at 50,000 rpm and 20 °C in a Beckman Optima-XL-A analytical ultracentrifuge, using 12 mm aluminium double sector centerpieces in an AN55Ti rotor. Scans were acquired in continuous mode at 280 nm, in the range of 0.1 to 1 absorption. At 20 °C, the partial specific volume of NiV PMD, solvent density and viscosity calculated with SEDNTERP (Laue et al., 1992), were 0.7333 mL/g, 1.00589 g/cm^3 and 0.01002 Ps, respectively. The data recorded from moving boundaries were analyzed in terms of both discrete species and continuous size distribution functions of sedimentation coefficient, $C(S)$, and molar mass, $C(M)$, using the program SEDFIT (Schuck and Rossmanith, 2000).

Equilibrium sedimentation experiments were performed at 4 °C with the same analytical ultracentrifuge in six channel centerpiece. Measurements were done at three successive speeds (10,000, 12,000 and 17,000 rpm) by taking scans at 280 and 257 nm, when sedimentation equilibrium was reached. High-sedimentation was conducted afterwards for baseline correction. At 4 °C, the partial specific volume of NiV PMD, solvent density and viscosity calculated with SEDNTERP, were 0.7264 mL/g, 1.00767 g/cm^3 and 0.01567 Ps, respectively. Average molecular speed masses were determined by fitting a sedimentation equilibrium model for a single solute to individual data sets with EQASSOC programs.

Far-UV circular dichroism (CD)

CD spectra were recorded on a Jasco 810 dichrograph using 1-mm thick quartz cells in 10 mM sodium phosphate pH 7 at 20 °C either in the absence or in the presence of increasing concentrations of 2,2,2 trifluoroethanol (TFE). CD spectra were measured between 185 and 260 nm, at 0.2 nm/min and were averaged from three independent acquisitions. Mean molar ellipticity values per residue (MRE) were calculated as $\mathrm{MRE} = 3300\ m\ \Delta A/(l\ c\ n)$, where l (path length) = 0.1 cm, n (number of residues) = 116, m (molecular mass in Daltons) = 13.475 and c (protein concentration in mg/mL) = 0.1. Spectra were deconvoluted using the DICHROWEB website

(http://dichroweb.cryst.bbk.ac.uk/html/home.shtml) which was supported by grants to the BBSRC Centre for Protein and Membrane Structure and Dynamics (CPMSD) (Whitmore and Wallace, 2004, 2008). The CONTINLL deconvolution method was used to estimate the α-helical content using the reference protein set 7.

In order to monitor protein unfolding, measurements at fixed wavelength (222 nm) were performed in the temperature range of 20–100 °C with data pitch 1 °C and a temperature slope of 1 °C/min. The buffer solution without the protein was used as blank. Fitting of experimental data was done using Sigmaplot.

Cross-linking experiments

A fixed amount of PMD (5 μg) was incubated for 20 h at 20 °C with increasing amounts (0–3.3 mM) of Suberic acid bis (*N*-hydroxysuccinimide ester) (SAB[1], Sigma) in 50 mM Hepes pH 7.0, 150 mM NaCl in a final volume of 30 μL. The reactions were quenched by adding 100 mM glycine. The samples were analyzed by 15% SDS-PAGE followed by Coomassie blue staining. SAB was first solubilized in DMSO at a concentration of 1% and then diluted in 50 mM Hepes pH 7.0, 150 mM NaCl to the desired concentration.

Small angle X-ray scattering (SAXS) measurements and ab initio 3D shape reconstructions

All small-angle X-ray scattering (SAXS) measurements were carried out at the ESRF on beamline BM29 at a working energy of 12.5 keV. The sample-to-detector distance of the X-rays was 2.847 m, leading to scattering vectors q ranging from 0.028 to 4.525 nm^{-1} (see Table 1 for details on data collection). The scattering vector is defined as $q=4\pi/\lambda\sin\theta$, where 2θ is the scattering angle. The exposure time was optimized to reduce radiation damage.

SAXS data were collected at 10 °C using samples of purified PMD (30 μL each) at the following concentrations: 1, 2.5 and 4 mg/mL in 20 mM Tris/HCl pH 8, 5 mM EDTA, 150 mM NaCl. Samples were loaded in a fully automated sample charger. Ten exposures of 10 s each were made for each protein concentration and data were combined to give the average scattering curve for each measurement. Any data points affected by aggregation, possibly induced by radiation damages were excluded. The profiles obtained at five different protein concentrations in the range 1–4 mg/mL had the same shape and were flat at low q values indicating the absence of significant aggregation. Then, we used the higher concentration (4 mg/mL) to obtain maximal information at high resolution.

Data reduction was performed using the established procedure available at BM29, and buffer background runs were subtracted from sample runs. The R_g and forward intensity at zero angle $I(0)$ were determined with the program PRIMUS (Konarev et al., 2003) according to the Guinier approximation at low values, in a $Q\times R_g$ range up to 1.3:

$$\mathrm{Ln}[I(Q)] = Ln[I_0] - \frac{Q^2R_g^2}{3} \quad (5)$$

The forward scattering intensity was calibrated using bovine serum albumin as reference. The R_g and pairwise distance distribution function, $P(r)$, were calculated with the program GNOM (Svergun, 1992). The maximum dimension (D_{max}) value was adjusted such that the R_g value obtained from GNOM agreed with that obtained from the Guinier analysis.

3D beads models were built by fitting the scattering data with the program DAMMIF (Franke and Svergun, 2009). This program restores a low-resolution shape of the protein as a volume filled with densely packed spheres that reproduces the experimental scattering curve by a simulated annealing minimization procedure. DAMMIF minimizes the interfacial area between the molecule and the solvent by imposing compactness and connectivity constraints. Twenty independents models were generated with DAMMIF either without imposing a symmetry or by imposing various symmetries. The models resulting from independent runs were superimposed using the DAMAVER suite (Volkov and Svergun, 2003). This yielded an initial alignment of structures based on their axes of inertia followed by minimization of the normalized spatial discrepancy (NSD), which is zero for identical objects and larger than one for systematically different objects. The aligned structures were then averaged, giving an effective occupancy to each voxel in the model, and filtered at half-maximal occupancy to produce models of the appropriate volume that were used for all subsequent analyses.

Structural modeling

Modeling was carried out using the SAM-T08 server that uses iterative hidden Markov model-based methods (HMMs) for constructing protein family profiles, using only sequence information (Karplus et al., 2003, 2005; Katzman et al., 2008). It is a fully automated method that generates a three-dimensional (3D) structural model by making use of a set of homologous structures. It is however not appropriate for modeling coiled-coil regions made up of several chains. Therefore, we first generated a model of a trimeric coiled-coil of 77 residues in length encompassing the region predicted as a coiled-coil (i.e. residues 513–578). This latter model was generated using the structure of hemagglutinin (pdb code 2HMG) as starting model. Then, using Chimera (Pettersen et al., 2004), we appended at the N-terminus of each of the three chains of the trimeric coiled-coil, the fragment encompassing residues 470–510, as found in the coordinates file generated by the SAM-T08 server. Note that this latter region corresponds to the NiV PMD N-terminal region not predicted to adopt a coiled-coil structure.

The dimeric model of NiV PMD was generated by aligning chains A and B of the trimeric model onto the dimeric coiled-coil structure of *Saccharomyces cerevisiae* Atg16e (pdb code 3A7O) using Chimera. The same approach was used to generate a tetrameric coiled-coil model using the SeV PMD tetrameric coiled-coil structure (pdb code 1EZJ) as a starting model.

All the models were subjected to 400 steps of steepest descent energy minimization using the GROMOS96 implementation of Swiss PDB Viewer (van Gunsteren et al., 1996).

Acknowledgments

We wish to thank Petra Pernot and Silvia Russi (ESRF) for their help in SAXS data collection, and Marion Sevajol and Eric Durand (AFMB) for their help in SAXS data collection and analysis. We are grateful to Alain Roussel (AFMB) for his help in building the model of a trimeric coiled-coil of 77 residues in length. We thank Christophe Flaudrops from the mass spectrometry platform of the IFR48 of Marseille for mass spectrometry analyses. S.L. thanks Martino Bolognesi (Universita' degli Studi of Milan) for co-supervising with her M.B.

Appendix A. Supporting information

Supplementary data associated with this article can be found in the online version at http://dx.doi.org/10.1016/j.virol.2013.07.031.

References

Albertini, A.A.V., Schoehn, G., Ruigrok, R.W., 2005. Structures impliquées dans la réplication et la transcription des virus à ARN non segmentés de sens négatif. Virologie 9, 83–92.

Assenberg, R., Delmas, O., Ren, J., Vidalain, P.O., Verma, A., Larrous, F., Graham, S.C., Tangy, F., Grimes, J.M., Bourhy, H., 2010. Structure of the nucleoprotein binding domain of Mokola virus phosphoprotein. J. Virol. 84, 1089–1096.

Belle, V., Rouger, S., Costanzo, S., Liquiere, E., Strancar, J., Guigliarelli, B., Fournel, A., Longhi, S., 2008. Mapping alpha-helical induced folding within the intrinsically disordered C-terminal domain of the measles virus nucleoprotein by site-directed spin-labeling EPR spectroscopy. Proteins: Struct. Funct. Bioinf. 73, 973–988.

Bernard, C., Gely, S., Bourhis, J.M., Morelli, X., Longhi, S., Darbon, H., 2009. Interaction between the C-terminal domains of N and P proteins of measles virus investigated by NMR. FEBS Lett. 583, 1084–1089.

Bischak, C.G., Longhi, S., Snead, D.M., Costanzo, S., Terrer, E., Londergan, C.H., 2010. Probing structural transitions in the intrinsically disordered C-terminal domain of the measles virus nucleoprotein by vibrational spectroscopy of cyanylated cysteines. Biophys. J. 99, 1676–1683.

Blanchard, L., Tarbouriech, N., Blackledge, M., Timmins, P., Burmeister, W.P., Ruigrok, R.W., Marion, D., 2004. Structure and dynamics of the nucleocapsid-binding domain of the Sendai virus phosphoprotein in solution. Virology 319, 201–211.

Blocquel, D., Bourhis, J.M., Eléouët, J.F., Gerlier, D., Habchi, J., Jamin, M., Longhi, S., Yabukarski, F., 2012a. Transcription et réplication des Mononégavirales: une machine moléculaire originale. Virologie 16, 225–257.

Blocquel, D., Habchi, J., Gruet, A., Blangy, S., Longhi, S., 2012b. Compaction and binding properties of the intrinsically disordered C-terminal domain of Henipavirus nucleoprotein as unveiled by deletion studies. Mol. Biosyst. 8, 392–410.

Bourhis, J., Johansson, K., Receveur-Bréchot, V., Oldfield, C.J., Dunker, A.K., Canard, B., Longhi, S., 2004. The C-terminal domain of measles virus nucleoprotein belongs to the class of intrinsically disordered proteins that fold upon binding to their physiological partner. Virus Res. 99, 157–167.

Bourhis, J.M., Receveur-Bréchot, V., Oglesbee, M., Zhang, X., Buccellato, M., Darbon, H., Canard, B., Finet, S., Longhi, S., 2005. The intrinsically disordered C-terminal domain of the measles virus nucleoprotein interacts with the C-terminal domain of the phosphoprotein via two distinct sites and remains predominantly unfolded. Protein Sci. 14, 1975–1992.

Bowden, T.A., Aricescu, A.R., Gilbert, R.J., Grimes, J.M., Jones, E.Y., Stuart, D.I., 2008a. Structural basis of Nipah and Hendra virus attachment to their cell-surface receptor ephrin-B2. Nat. Struct. Mol. Biol. 15, 567–572.

Bowden, T.A., Crispin, M., Harvey, D.J., Aricescu, A.R., Grimes, J.M., Jones, E.Y., Stuart, D.I., 2008b. Crystal structure and carbohydrate analysis of Nipah virus attachment glycoprotein: a template for antiviral and vaccine design. J. Virol. 82, 11628–11636.

Bowden, T.A., Crispin, M., Harvey, D.J., Jones, E.Y., Stuart, D.I., 2010. Dimeric architecture of the Hendra virus attachment glycoprotein: evidence for a conserved mode of assembly. J. Virol. 84, 6208–6217.

Chan, Y.P., Koh, C.L., Lam, S.K., Wang, L.F., 2004. Mapping of domains responsible for nucleocapsid protein–phosphoprotein interaction of Henipaviruses. J. Gen. Virol. 85, 1675–1684.

Chouard, T., 2011. Structural biology: breaking the protein rules. Nature 471, 151–153.

Communie, G., Crepin, T., Maurin, D., Ringkjobing Jensen, M., Blackledge, M., Ruigrok, R.W., 2013. Structure of the tetramerization domain of measles virus phosphoprotein. J. Virol..

Cox, R., Green, T.J., Purushotham, S., Deivanayagam, C., Bedwell, G.J., Prevelige, P.E., Luo, M., 2013. Structural and functional characterization of the Mumps virus phosphoprotein. J. Virol..

Curran, J., Kolakofsky, D., 1999. Replication of paramyxoviruses. Adv. Virus Res. 54, 403–422.

DeLano, W.L., 2002. The PyMOL molecular graphics system. Funct. Bioinf. 30, 442–454.

Delmas, O., Assenberg, R., Grimes, J.M., Bourhy, H., 2010. The structure of the nucleoprotein binding domain of lyssavirus phosphoprotein reveals a structural relationship between the N-RNA binding domains of Rhabdoviridae and Paramyxoviridae. RNA Biol. 7, 322–327.

Ding, H., Green, T.J., Lu, S., Luo, M., 2006. Crystal structure of the oligomerization domain of the phosphoprotein of vesicular stomatitis virus. J. Virol. 80, 2808–2814.

Dunker, A.K., Oldfield, C.J., Meng, J., Romero, P., Yang, J.Y., Chen, J.W., Vacic, V., Obradovic, Z., Uversky, V.N., 2008a. The unfoldomics decade: an update on intrinsically disordered proteins. BMC Genom. 9 (Suppl. 2), S1.

Dunker, A.K., Silman, I., Uversky, V.N., Sussman, J.L., 2008b. Function and structure of inherently disordered proteins. Curr. Opin. Struct. Biol. 18, 756–764.

Eaton, B.T., Mackenzie, J.S., Wang, L.F., 2007. Henipaviruses. In: Fields, B.N., Knipe, D. M., Howley, P.M. (Eds.), Fields Virology, fifth ed. Lippincott-Raven, Philadelphia, pp. 1587–1600.

Ferron, F., Rancurel, C., Longhi, S., Cambillau, C., Henrissat, B., Canard, B., 2005. VaZyMolO: a tool to define and classify modularity in viral proteins. J. Gen. Virol. 86, 743–749.

Franke, D., Svergun, D.I., 2009. DAMMIF, a program for rapid ab-initio shape determination in small-angle scattering. J. Appl. Crystallogr. 42, 342–346.

Gely, S., Lowry, D.F., Bernard, C., Ringkjobing-Jensen, M., Blackledge, M., Costanzo, S., Darbon, H., Daughdrill, G.W., Longhi, S., 2010. Solution structure of the C-terminal X domain of the measles virus phosphoprotein and interaction with the intrinsically disordered C-terminal domain of the nucleoprotein. J. Mol. Recognit. 23, 435–447.

Habchi, J., Blangy, S., Mamelli, L., Ringkjobing Jensen, M., Blackledge, M., Darbon, H., Oglesbee, M., Shu, Y., Longhi, S., 2011. Characterization of the interactions between the nucleoprotein and the phosphoprotein of Henipaviruses. J. Biol. Chem. 286, 13583–13602.

Habchi, J., Mamelli, L., Darbon, H., Longhi, S., 2010. Structural disorder within Henipavirus nucleoprotein and phosphoprotein: from predictions to experimental assessment. PLoS One 5, e11684.

Houben, K., Marion, D., Tarbouriech, N., Ruigrok, R.W., Blanchard, L., 2007. Interaction of the C-terminal domains of sendai virus N and P proteins: comparison of polymerase–nucleocapsid interactions within the paramyxovirus family. J. Virol. 81, 6807–6816.

Ivanov, I., Crepin, T., Jamin, M., Ruigrok, R.W., 2010. Structure of the dimerization domain of the rabies virus phosphoprotein. J. Virol. 84, 3707–3710.

Jacob, Y., Real, E., Tordo, N., 2001. Functional interaction map of lyssavirus phosphoprotein: identification of the minimal transcription domains. J. Virol. 75, 9613–9622.

Jensen, M.R., Bernado, P., Houben, K., Blanchard, L., Marion, D., Ruigrok, R.W., Blackledge, M., 2010. Structural disorder within sendai virus nucleoprotein and phosphoprotein: insight into the structural basis of molecular recognition. Protein Pept. Lett. 17, 952–960.

Johansson, K., Bourhis, J.M., Campanacci, V., Cambillau, C., Canard, B., Longhi, S., 2003. Crystal structure of the measles virus phosphoprotein domain responsible for the induced folding of the C-terminal domain of the nucleoprotein. J. Biol. Chem. 278, 44567–44573.

Karlin, D., Ferron, F., Canard, B., Longhi, S., 2003. Structural disorder and modular organization in Paramyxovirinae N and P. J. Gen. Virol. 84, 3239–3252.

Karplus, K., Karchin, R., Draper, J., Casper, J., Mandel-Gutfreund, Y., Diekhans, M., Hughey, R., 2003. Combining local-structure, fold-recognition, and new fold methods for protein structure prediction. Proteins 53 (Suppl. 6), 491–496.

Karplus, K., Katzman, S., Shackleford, G., Koeva, M., Draper, J., Barnes, B., Soriano, M., Hughey, R., 2005. SAM-T04: what is new in protein-structure prediction for CASP6. Proteins 61 (Suppl. 7), 135–142.

Katzman, S., Barrett, C., Thiltgen, G., Karchin, R., Karplus, K., 2008. PREDICT-2ND: a tool for generalized protein local structure prediction. Bioinformatics 24, 2453–2459.

Kavalenka, A., Urbancic, I., Belle, V., Rouger, S., Costanzo, S., Kure, S., Fournel, A., Longhi, S., Guigliarelli, B., Strancar, J., 2010. Conformational analysis of the partially disordered measles virus N_{TAIL}-XD complex by SDSL EPR spectroscopy. Biophys. J. 98, 1055–1064.

Kingston, R.L., Gay, L.S., Baase, W.S., Matthews, B.W., 2008. Structure of the nucleocapsid-binding domain from the mumps virus polymerase; an example of protein folding induced by crystallization. J. Mol. Biol. 379, 719–731.

Kolakofsky, D., Le Mercier, P., Iseni, F., Garcin, D., 2004. Viral DNA polymerase scanning and the gymnastics of Sendai virus RNA synthesis. Virology 318, 463–473.

Konarev, P.V., Volkov, V.V., Sokolova, A.V., Koch, M.H.J., Svergun, D.I., 2003. PRIMUS: a Windows PC-based system for small-angle scattering data analysis. J. Appl. Crystallogr. 36, 1277–1282.

Lamb, R.A., Parks, G.D., 2007. Paramyxoviridae: the viruses and their replication. In: Knipe, D.M., Howley, P.M. (Eds.), Fields Virology, fifth ed. Lippincott Williams & Wilkins, Philadelphia, PA, pp. 1450–1497.

Lau, S.Y., Taneja, A.K., Hodges, R.S., 1984. Synthesis of a model protein of defined secondary and quaternary structure. Effect of chain length on the stabilization and formation of two-stranded alpha-helical coiled-coils. J. Biol. Chem. 259, 13253–13261.

Laue, T.M., Shah, B.D., Ridgeway, T.M., Pelletier, S.L., 1992. In: Harding, S.E., Rowe, A. J., Horton, J.C. (Eds.), Computer-aided Interpretation of Analytical Sedimentation Data for Proteins in Analytical Ultracentrifugation. Biochemistry and Polymer Sciences Royal Society of Chemistry, Cambridge, UK, pp. 90–125.

Leyrat, C., Gerard, F.C., de Almeida Ribeiro Jr., E., Ivanov, I., Ruigrok, R.W., Jamin, M., 2010. Structural disorder in proteins of the rhabdoviridae replication complex. Protein Pept. Lett. 17, 979–987.

Llorente, M.T., Barreno-Garcia, B., Calero, M., Camafeita, E., Lopez, J.A., Longhi, S., Ferron, F., Varela, P.F., Melero, J.A., 2006. Structural analysis of the human respiratory syncitial virus phosphoprotein: characterization of an α-helical domain involved in oligomerization. J. Gen. Virol. 87, 159–169.

Llorente, M.T., Taylor, I.A., Lopez-Vinas, E., Gomez-Puertas, P., Calder, L.J., Garcia-Barreno, B., Melero, J.A., 2008. Structural properties of the human respiratory syncytial virus P protein: evidence for an elongated homotetrameric molecule that is the smallest orthologue within the family of paramyxovirus polymerase cofactors. Proteins 72, 946–958.

Longhi, S., Receveur-Brechot, V., Karlin, D., Johansson, K., Darbon, H., Bhella, D., Yeo, R., Finet, S., Canard, B., 2003. The C-terminal domain of the measles virus nucleoprotein is intrinsically disordered and folds upon binding to the C-terminal moiety of the phosphoprotein. J. Biol. Chem. 278, 18638–18648.

Lou, Z., Xu, Y., Xiang, K., Su, N., Qin, L., Li, X., Gao, G.F., Bartlam, M., Rao, Z., 2006. Crystal structures of Nipah and Hendra virus fusion core proteins. FEBS J. 273, 4538–4547.

Lupas, A.N., Gruber, M., 2005. The structure of alpha-helical coiled coils. Adv. Protein Chem. 70, 37–78.

Marsh, G.A., de Jong, C., Barr, J.A., Tachedjian, M., Smith, C., Middleton, D., Yu, M., Todd, S., Foord, A.J., Haring, V., Payne, J., Robinson, R., Broz, I., Crameri, G., Field, H.E., Wang, L.F., 2012. Cedar virus: a novel Henipavirus isolated from Australian bats. PLoS Pathog. 8, e1002836.

Martinho, M., Habchi, J., El Habre, Z., Nesme, L., Guigliarelli, B., Belle, V., Longhi, S., 2013. Assessing induced folding within the intrinsically disordered C-terminal domain of the Henipavirus nucleoproteins by site directed spin labeling EPR spectroscopy. J. Biomol. Struct. Dyn. 1, 453–471.

Mavrakis, M., McCarthy, A.A., Roche, S., Blondel, D., Ruigrok, R.W., 2004. Structure and function of the C-terminal domain of the polymerase cofactor of rabies virus. J. Mol. Biol. 343, 819–831.
Morin, B., Bourhis, J.M., Belle, V., Woudstra, M., Carrière, F., Guigliarelli, B., Fournel, A., Longhi, S., 2006. Assessing induced folding of an intrinsically disordered protein by site-directed spin-labeling EPR spectroscopy. J. Phys. Chem. B 110, 20596–20608.
Omi-Furutani, M., Yoneda, M., Fujita, K., Ikeda, F., Kai, C., 2010. Novel phosphoprotein-interacting region in Nipah virus nucleocapsid protein and its involvement in viral replication. J. Virol. 84, 9793–9799.
Pettersen, E.F., Goddard, T.D., Huang, C.C., Couch, G.S., Greenblatt, D.M., Meng, E.C., Ferrin, T.E., 2004. UCSF Chimera—a visualization system for exploratory research and analysis. J. Comput. Chem. 25, 1605–1612.
Rahaman, A., Srinivasan, N., Shamala, N., Shaila, M.S., 2004. Phosphoprotein of the rinderpest virus forms a tetramer through a coiled coil region important for biological function. A structural insight. J. Biol. Chem. 279, 23606–23614.
Ribeiro Jr., E.A., Favier, A., Gerard, F.C., Leyrat, C., Brutscher, B., Blondel, D., Ruigrok, R.W., Blackledge, M., Jamin, M., 2008. Solution structure of the C-terminal nucleoprotein-RNA binding domain of the vesicular stomatitis virus phosphoprotein. J. Mol. Biol. 382, 525–538.
Ringkjøbing Jensen, M., Communie, G., Ribeiro Jr., E.D., Martinez, N., Desfosses, A., Salmon, L., Mollica, L., Gabel, F., Jamin, M., Longhi, S., Ruigrok, R.W., Blackledge, M., 2011. Intrinsic disorder in measles virus nucleocapsids. Proc. Nat. Acad. Sci. U.S.A. 108, 9839–9844.
Roux, L., 2005. Dans le génome des Paramyxovirinae, les promoteurs et leurs activités sont façonnés par la ≪ règle de six. Virologie 9, 19–34.
Schuck, P., Rossmanith, P., 2000. Determination of the sedimentation coefficient distribution by least-squares boundary modeling. Biopolymers 54, 328–341.
Svergun, D., 1992. Determination of the regularization parameters in indirect-trasform methods using perceptual criteria. J. Appl. Crystallogr. 25, 495–503.
Svergun, D., Barberato, C., Koch, M.H.J., 1995. CRYSOL, a program to evaluate X-ray solution scattering of biological macromolecules from atomic coordinates. J. Appl. Crystallogr. 28, 768–773.
Tarbouriech, N., Curran, J., Ebel, C., Ruigrok, R.W., Burmeister, W.P., 2000a. On the domain structure and the polymerization state of the sendai virus P protein. Virology 266, 99–109.
Tarbouriech, N., Curran, J., Ruigrok, R.W., Burmeister, W.P., 2000b. Tetrameric coiled coil domain of Sendai virus phosphoprotein. Nat. Struct. Biol. 7, 777–781.
Turoverov, K.K., Kuznetsova, I.M., Uversky, V.N., 2010. The protein kingdom extended: ordered and intrinsically disordered proteins, their folding, supramolecular complex formation, and aggregation. Prog. Biophys. Mol. Biol. 102, 73–84.
Uversky, V.N., 2002. What does it mean to be natively unfolded? Eur. J. Biochem. 269, 2–12.
Uversky, V.N., 2010. The mysterious unfoldome: structureless, underappreciated, yet vital part of any given proteome. J. Biomed. Biotechnol. 2010, 568068.
Uversky, V.N., 2013. A decade and a half of protein intrinsic disorder: biology still waits for physics. Protein Sci. 22, 693–724.
Uversky, V.N., Dunker, A.K., 2010. Understanding protein non-folding. Biochim. Biophys. Acta 1804, 1231–1264.
van Gunsteren, W.F., Billeter, S.R., Eising, A.A., Hünenberger, P.H., Krüger, P., Mark, A.E., Scott, W.R.P., Tironi, I.G., 1996. Biomolecular Simulation: the GROMOS96 Manual and User Guide. vdf Hochschuverlag. Zürich, Switzerland.
Volkov, V.V., Svergun, D.I., 2003. Uniqueness of ab initio shape determination in small-angle scattering. J. Appl. Crystallogr. 36, 860–864.
Wang, L.F., Yu, M., Hansson, E., Pritchard, L.I., Shiell, B., Michalski, W.P., Eaton, B.T., 2000. The exceptionally large genome of Hendra virus: support for creation of a new genus within the family Paramyxoviridae. J. Virol. 74, 9972–9979.
Whitmore, L., Wallace, B.A., 2004. DICHROWEB, an online server for protein secondary structure analyses from circular dichroism spectroscopic data. Nucleic Acids Res. 32, W668–W673.
Whitmore, L., Wallace, B.A., 2008. Protein secondary structure analyses from circular dichroism spectroscopy: methods and reference databases. Biopolymers 89, 392–400.
Wilkins, D.K., Grimshaw, S.B., Receveur, V., Dobson, C.M., Jones, J.A., Smith, L.J., 1999. Hydrodynamic radii of native and denatured proteins measured by pulse field gradient NMR techniques. Biochemistry 38, 16424–16431.